Tensor of the second-order nonlinear susceptibility in asymmetrically strained silicon waveguides: analysis and experimental validation

Matthew W. Puckett,* Joseph S. T. Smalley, Maxim Abashin, Andrew Grieco, and Yeshaiahu Fainman

Department of Electrical & Computer Engineering, University of California, San Diego, 9500 Gilman Dr, La Jolla, California 92023, USA

**Corresponding author: mwpucket@ucsd.edu*

Received January 14, 2014; revised February 11, 2014; accepted February 11, 2014;
posted February 12, 2014 (Doc. ID 204743); published March 14, 2014

We theoretically consider the existence of multiple nonzero components of the second-order nonlinear susceptibility tensor, $\chi^{(2)}$, generated via strain-induced symmetry breaking in crystalline silicon. We determine that, in addition to the previously reported $\chi^{(2)}_{xxy}$ component, the $\chi^{(2)}_{yyy}$ component also becomes nonzero based on the remaining symmetry present in the strained material. In order to characterize these two nonlinearities, we fabricate Fabry–Perot waveguide resonators on 250 nm thick silicon-on-insulator wafers clad with 180 nm of compressively stressed (−1.275 GPa) silicon nitride. We measure the shifts in these devices' modal effective indices in response to several bias electric fields and calculate the $\chi^{(2)}_{\mathrm{eff},xxy}$ and $\chi^{(2)}_{\mathrm{eff},yyy}$ nonlinear susceptibility tensor elements induced by the breaking of the guiding material's inversion symmetry. Through the incorporation of finite element simulations encompassing the theoretical distribution of strain, the applied bias field, and the optical modes supported by the waveguide geometry, we extract two phenomenological scaling coefficients which relate the induced optical nonlinearities to the local strain gradient.

OCIS codes: (050.0050) Diffraction and gratings; (190.0190) Nonlinear optics; (000.4430) Numerical approximation and analysis; (160.2100) Electro-optical materials.

http://dx.doi.org/10.1364/OL.39.001693

Lithium niobate is the most commonly used material for optical modulation due to its high second-order nonlinear susceptibility of 360 pm/V [1], its fast response time, and the wide range of waveguide configurations it supports. However, lithium niobate modulators suffer from several considerable limitations, including high substrate cost, large physical footprint, and difficulty of integration with the silicon-on-insulator (SOI) material platform commonly used in photonics and microelectronics. Therefore, it is desirable to create comparable linear electro-optic effects in an SOI-platform through CMOS-compatible fabrication processes. Several unique methods have been pursued to this end [2–4], but currently, none simultaneously meet all of the strenuous requirements needed for an implementation in telecommunication applications.

More recently, strained silicon has become a subject of great interest within the field of nonlinear optics. Through the breaking of crystalline silicon's inversion symmetry via physical strain, a nonzero $\chi^{(2)}_{xxy}$ component of the second-order nonlinear susceptibility tensor may be generated and exploited in such nonlinear optical processes as second-harmonic generation and linear electro-optic modulation. This effect was first demonstrated by Jacobsen *et al.* in 2006 [5], and the initial discovery has since been expanded upon by a number of research groups [6–8].

The highest nonlinearity generated in a strained silicon waveguide is $\chi^{(2)}_{xxy} = 190$ pm/V; this value was reported by Chmielak *et al.* in 2013 [9]. The local optical nonlinearity is known to be linearly proportional to the gradient of the induced strain, and the impressive value reported in the literature was achieved by maximizing the strain gradient near the waveguide sidewalls.

Initial theories have asserted that a net electric field is induced by the displacement of bound charge, and attempts based upon this theory have been made to theoretically relate the strain gradient to the magnitude of the optical nonlinearity [10]. These efforts have highlighted a discrepancy of approximately 3 orders of magnitude between theoretically predicted and experimentally observed values. *Ab initio* models have demonstrated how the displacement of atoms leads to nonlinear effects through time-dependent density functional theory [6], but these models have not as of yet provided an explicit relationship between local strain gradients and the induced nonlinear optical response.

Until modifications can be made to existing theoretical models, or until entirely new models are established, the extraction of a phenomenological scaling coefficient relating the local strain gradient to the optical nonlinearity will be advantageous in the design and characterization of devices incorporating strained silicon.

In this manuscript, we consider the breaking of crystalline symmetry through strain on the scale of a single unit cell of crystalline silicon. Through observation of the remaining symmetries present in the cell, we determine which components of the strain-induced $\chi^{(2)}$ tensor are not identically required to be equal to zero. Through this analysis we find that, in addition to the previously observed $\chi^{(2)}_{xxy}$, there are three other unique tensor components that are generated: $\chi^{(2)}_{yyy}$, $\chi^{(2)}_{xyz}$, and $\chi^{(2)}_{zzy}$. These three tensor components are predicted to be nonzero in the presence of a gradient of x or z-oriented strain along the y direction, with the coordinate axes defined in Fig. 1.

To verify our predictions, we fabricate Fabry–Perot resonators on 250 nm thick SOI wafers [11] and clad them with 180 nm of compressively stressed silicon nitride. By applying bias electric fields vertically across the waveguide, we extract the waveguides' effective nonlinear coefficients $\chi^{(2)}_{\mathrm{eff},xxy}$ and $\chi^{(2)}_{\mathrm{eff},yyy}$, in addition to $\chi^{(3)}_{\mathrm{eff},xxyy}$ and $\chi^{(3)}_{\mathrm{eff},yyyy}$. Then, we use finite element models

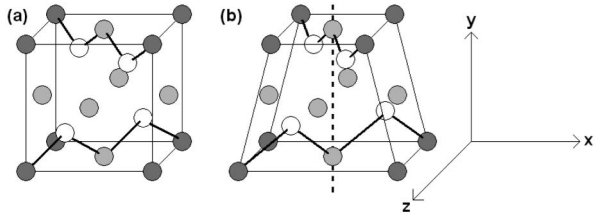

Fig. 1. (a) A single unit cell of silicon in the absence of strain, showing a few bonds to illustrate the relative locations of atoms within the cell. (b) A single unit cell of silicon in the presence of a y-oriented gradient of x-oriented strain, demonstrating the loss of centrosymmetry and the existence of rotational symmetry of 180° about the dashed line.

to determine scaling coefficients which relate the local strain gradient in silicon to each of the two measured $\chi^{(2)}$ tensor components, aiding in the design and characterization of future optical devices composed of strained silicon. Our approach may be expanded upon in the future to determine the most advantageous implementations of strain relative to silicon's crystallographic orientation.

The derivation of the interrelationships among the 27 components of a nonspecific tensor of rank three through the analysis of a material's symmetry is a well-established process [12]. To the best of our knowledge, this technique has not yet been explicitly applied to strained silicon. In the following, we use this method to predict the existence of tensor components not yet reported in the literature.

Consider a unit cell of crystalline silicon, shown in Fig. 1(a). The lattice is centrosymmetric, which means the x, y, and z axes may all be inverted about a given point without moving any of the silicon atoms into positions which were not previously occupied. The transformation matrix corresponding to the inversion operation is given by

$$M_{\text{symm}} = [-1 \quad 0 \quad 0; \quad 0 \quad -1 \quad 0; \quad 0 \quad 0 \quad -1]. \qquad (1a)$$

Because performing this transformation leaves the material unchanged, it is required that all of the material's physical properties be invariant under the transformation. By enforcing that the third rank $\chi^{(2)}$ tensor be unchanged by the centrosymmetry transformation, it is straightforward to conclude that every element of the tensor must equal zero. This is consistent with the well-known fact that centrosymmetric materials do not exhibit the Pockels effect.

However, asymmetric strain removes the unit cell's centrosymmetry, as shown in Fig. 1(b); inverting about all three axes will clearly place atoms in positions that were not previously occupied. The symmetry that still remains, however, is rotational symmetry of 180° about the y axis. This new transformation may be represented by a second matrix, given as

$$M_{\text{asymm}} = [-1 \quad 0 \quad 0; \quad 0 \quad 1 \quad 0; \quad 0 \quad 0 \quad -1]. \qquad (1b)$$

Again enforcing that the $\chi^{(2)}$ tensor be unchanged by the transformation matrix, we now find that several components of the $\chi^{(2)}$ tensor are not identically equal to zero. These components are $\chi^{(2)}_{xxy}$, $\chi^{(2)}_{yyy}$, $\chi^{(2)}_{zzy}$, $\chi^{(2)}_{xyz}$, and all of their index permutations.

The existence of a nonzero $\chi^{(2)}_{xxy}$ coefficient has been of particular interest in the context of linear optical modulation, as it allows the effective index of a TE-like mode to change linearly in response to a vertically applied electric field. The $\chi^{(2)}_{yyy}$ component is noteworthy as well, as it allows for the same type of modulation if a TM-like mode is considered instead.

In order to experimentally validate the existence of the $\chi^{(2)}_{xxy}$ and $\chi^{(2)}_{yyy}$ tensor coefficients, we fabricated Fabry–Perot waveguide resonators on SOI wafers consisting of 250 nm thick silicon layers. The waveguides were 450 nm wide, and the grating periods chosen for the TE- and TM-like modes were 312 and 376 nm, respectively. The cavity lengths were chosen to be 100 μm, ensuring that many cavity resonances would be contained within the transmission spectra's stop bands. Each of the Bragg mirrors was made using 70 grating periods to assure sufficiently high reflectivity.

To fabricate our waveguides, we first spun hydrogen silsesquioxane onto SOI wafers. We then used electron beam lithography and reactive ion etching to etch the pattern of our waveguides into the wafers. Next, we used plasma-enhanced chemical vapor deposition (PECVD) to clad the waveguides with 180 nm of amorphous silicon nitride. By selectively generating only lower frequency plasmas during the PECVD process, we were able to produce a compressive stress within the silicon nitride layer of −1.275 GPa. The silicon nitride layer did not extend continuously over the waveguide, but was instead separated into discrete layers, as shown in Fig. 2.

Next, we deposited 1020 nm of amorphous silica on top of the nitride layer, also through PECVD. To create electrodes, we sputtered 1.2 μm of gold over the entire sample, using a thin layer of titanium as an adhesion layer. When applying a voltage across our waveguides, the gold layer served as the top electrical contact, whereas the silicon substrate of the SOI wafer was used as the bottom contact. The resulting waveguide cross section is shown in Fig. 3(a), and the device layout is illustrated in Fig. 3(b). As a result of scanning electron microscopy done throughout the fabrication process, the waveguide cross sections were known to a high degree of accuracy.

The passive transmission spectra for the fabricated devices are shown in Fig. 4. For the TE-like mode, we obtained a stop band centered at 1540 nm, whereas for the TM-like mode it was centered at 1537 nm. Respectively,

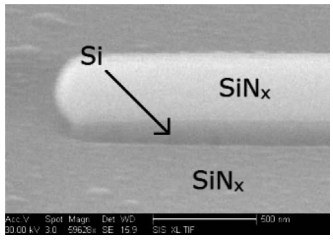

Fig. 2. ESEM side view of the edge of a 250 nm tall waveguide clad with 180 nm of silicon nitride through PECVD. Two distinct regions have formed. One comes in contact with the top surface of the waveguide, whereas the other grows on the substrate.

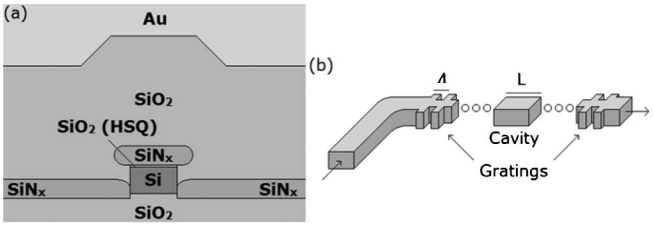

Fig. 3. (a) Waveguide cross section resulting from the outlined fabrication process. (b) The device outline showing, from left to right, the input facet, a 90° bend, the cavity located between two Bragg mirrors, and the output facet.

these stop band locations correspond to modal effective indices of 2.468 and 2.044.

By applying bias voltages across the gold film and the silicon substrate, we were able to induce vertical electric fields across the waveguides. Theoretically, the average electric field within the waveguide resulting from an applied voltage of +1 V was calculated to be $E_{y,\mathrm{avg}} = -5.87\mathrm{e}4\ \mathrm{Vm}^{-1}$.

The estimated Q-factors of the cavity resonances were 1500 for the TE-like mode and 750 for the TM-like mode, corresponding to FWHM of ~1 nm and ~2 nm, respectively. There were smaller resonances superimposed over the fundamental ones, which were caused by reflections occurring at the waveguide end facets due to impedance mismatches.

In order to measure the Pockels effect, we chose one resonance for each of the two waveguides, then measured the changes in the these resonances' peak wavelengths that resulted from the application of voltages ranging from −50 V to +50 V. These resonance shifts were then related to changes in the modal effective indices through the simple equation

$$\Delta n = \frac{n}{\lambda}\Delta\lambda. \tag{2}$$

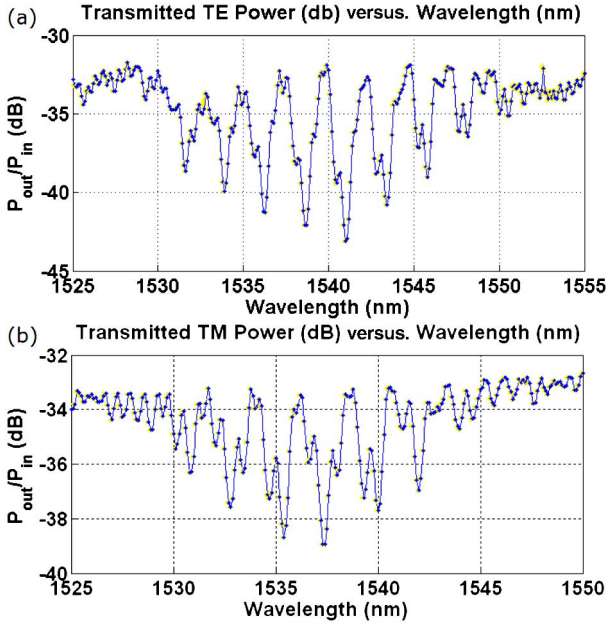

Fig. 4. Transmission spectra of the (a) TE- and (b) TM-like modes, in the absence of an applied voltage.

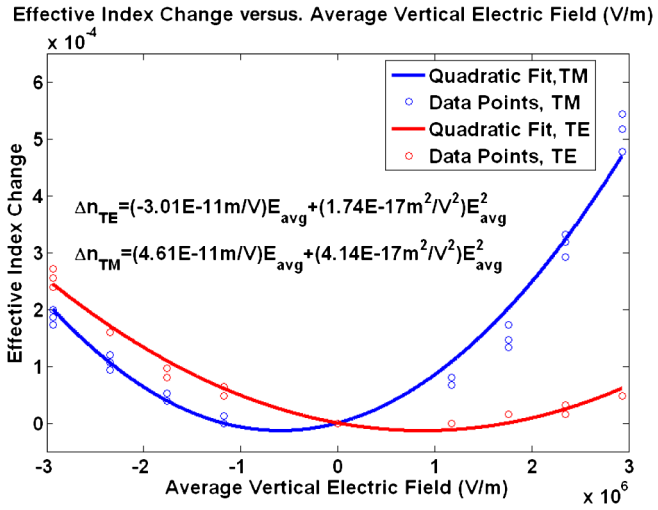

Fig. 5. Observed index changes of the TE- and TM-like modes' resonances in response to applied voltages ranging from −50 V to +50 V.

For the TE- and TM-like modes, the chosen resonances were centered at wavelengths of 1542.175 and 1536.110 nm, respectively.

Because the waveguides possessed third-order optical nonlinearities in addition to the second-order nonlinearities of interest, the modes' effective indices varied quadratically with respect to the applied voltage. By fitting our measured index shifts to a quadratic curve, we were able to extract both the second- and third-order nonlinearities for each mode. The experimental data and the fitted curves are both shown in Fig. 5. We used the following expressions to relate our observed index shifts to the second- and third-order nonlinearities:

$$\Delta n_{\mathrm{eff,TE}} = \frac{\chi^{(2)}_{\mathrm{eff},xxy}E_{\mathrm{avg}}}{n_{\mathrm{eff,TE}}} + \frac{3\chi^{(3)}_{\mathrm{eff},xxyy}E^2_{\mathrm{avg}}}{2n_{\mathrm{eff,TE}}}, \tag{3a}$$

$$\Delta n_{\mathrm{eff,TM}} = \frac{\chi^{(2)}_{\mathrm{eff},yyy}E_{\mathrm{avg}}}{2n_{\mathrm{eff,TM}}} + \frac{\chi^{(2)}_{\mathrm{eff},yyyy}E^2_{\mathrm{avg}}}{2n_{\mathrm{eff,TM}}}. \tag{3b}$$

In these equations, E_{avg} is the average vertical bias electric field within the silicon portion of the waveguide cross section. From the trend lines shown in Fig. 5, we obtained the following values for our waveguides' nonlinear susceptibility components: $\chi^{(2)}_{\mathrm{eff},xxy} = (-74 \pm 3)$ pm/V, $\chi^{(2)}_{\mathrm{eff},yyy} = (188 \pm 6)$ pm/V, $\chi^{(3)}_{\mathrm{eff},xxyy} = (2.9\mathrm{e}-17 \pm 2\mathrm{e}-18)\ \mathrm{m}^2/\mathrm{V}^2$, and $\chi^{(3)}_{\mathrm{eff},yyyy} = (1.7\mathrm{e}-16 \pm 7\mathrm{e}-18)\ \mathrm{m}^2/\mathrm{V}^2$.

In order to determine the coefficients relating the strain gradient to the second-order optical nonlinearities, we enforced the condition that an applied bias voltage, chosen to be too small to interact significantly with the third-order nonlinearities, must lead to shifts in the modal effective indices that match our generated trend lines. We required that the local refractive index within the silicon waveguide vary with the stress, the strain gradient, and the local electric field as

$$\Delta n_{x,Si} = -C_1 s_{xx} - C_2(s_{yy} + s_{zz}) + \frac{C_{xxy}\left(\frac{de_{xx}}{dy}\right)E_y}{n_{x,Si}}, \quad (4a)$$

$$\Delta n_{y,Si} = -C_1 s_{yy} - C_2(s_{xx} + s_{zz}) + \frac{C_{yyy}\left(\frac{de_{xx}}{dy}\right)E_y}{2n_{x,Si}}, \quad (4b)$$

where C_1 and C_2 are the first and second stress optical coefficients of silicon, respectively, s_{xx}, s_{yy}, and s_{zz} are the components of stress within silicon, e_{xx} is the x-oriented component of strain within silicon, and C_{xxy} and C_{yyy} are the unknown scaling coefficients of interest for $\chi^{(2)}_{xxy}$ and $\chi^{(2)}_{yyy}$, respectively, such that

$$\chi^{(2)}_{xxy} = C_{xxy}\left(\frac{de_{xx}}{dy}\right), \quad (5a)$$

$$\chi^{(2)}_{yyy} = C_{yyy}\left(\frac{de_{xx}}{dy}\right). \quad (5b)$$

The first and second stress optical coefficients of silicon were taken to be −11.35e − 12 Pa^{-1} and 3.65e − 12 Pa^{-1}, respectively [13], and the stress, strain, and electric field values were taken from our finite element model analysis.

An applied voltage of +1 V changes the effective index of the TE- and TM-like modes by $1.77\text{e}-6 \pm 8\text{e}-8$ and $-2.71\text{e}-6 \pm 8\text{e}-8$, respectively. These changes are achieved when C_{xxy} equals $(-5.89\text{e}-15 \pm 2.4\text{e}-16)$ m^2/V and C_{yyy} equals $(3.06\text{e}-14 \pm 9.8\text{e}-16)$ m^2/V. It should be noted that any uncertainties in the initial distribution of stress within the silicon nitride layer will lead to increased variability in the reported scaling coefficients. Although deviations from the mean thin film stress of −1.275 GPa are assumed to be negligible, the resulting uncertainties are not readily quantified.

The highest local nonlinearities are found to exist near two edges where the silicon nitride comes into contact with the waveguide sidewalls. There is an additional nonlinearity resulting from the upper nitride layer straining the top of waveguide, but this effect is comparatively negligible. The effective nonlinearity resulting from the strain gradient is anticipated to increase as the waveguide width is decreased, resulting in a larger overlap between the optical mode and the higher local nonlinearities. This effect has been observed experimentally in previous works [9].

The proportionality constants relevant to wave-mixing applications are not expected to be equivalent to the ones given here, and should be independently measured through such techniques as phase-matched second-harmonic generation [6].

We have shown that, in addition to the well-known $\chi^{(2)}_{xxy}$, which is generated by the breaking of centrosymmetry in strained silicon, there also exists a nonzero $\chi^{(2)}_{yyy}$. The existence of this second value is critical because it enables strained silicon waveguides to modulate both TE- and TM-like modes.

Additionally, we have extracted phenomenological coefficients which relate the locally induced nonlinearities in strained silicon to the local strain gradient. In the future, knowledge of these relationships will allow the effective nonlinear coefficients of strained silicon waveguides to be more accurately predicted prior to fabrication. If properly utilized, this capability will be beneficial in the design of highly efficient optical modulators and optical wave mixers.

This work was supported by the Defense Advanced Research Projects Agency (DARPA), the National Science Foundation (NSF), the NSF ERC CIAN, the Office of Naval Research (ONR), the Multidisciplinary University Research Initiative (MURI), and the Cymer Corporation.

References

1. G. Li and P. Yu, J. Lightwave Technol. **21**, 2010 (2003).
2. P. Dong, S. Liao, D. Feng, H. Liang, D. Zheng, R. Shafiiha, C. Kung, W. Qian, G. Li, X. Zheng, A. Krishnamoorthy, and M. Asghari, Opt. Express **17**, 22484 (2009).
3. X. Zheng, J. Lexau, Y. Luo, H. Thacker, T. Pinguet, A. Mekis, G. Li, J. Shi, P. Amberg, N. Pinckney, K. Raj, R. Ho, J. Cunningham, and A. Krishnamoorthy, Opt. Express **18**, 3059 (2010).
4. G. Reed, G. Mashanovich, F. Gardes, and D. Thomson, Nat. Photonics **4**, 518 (2010).
5. R. Jacobsen, K. Andersen, P. Borel, J. Fage-Pedersen, L. Frandsen, O. Hansen, M. Kristensen, A. Lavrinenko, G. Moulin, H. Ou, C. Peucheret, B. Zsigri, and A. Bjarklev, Nature **441**, 199 (2006).
6. M. Cazzanelli, F. Bianco, E. Borga, G. Pucker, M. Ghulinyan, E. Degoli, E. Luppi, V. Véniard, S. Ossicini, D. Modotto, S. Wabnitz, R. Pierobon, and L. Pavesi, Nat. Mater. **11**, 148 (2011).
7. I. Avrutsky and R. Soref, Opt. Express **19**, 21707 (2011).
8. B. Chmielak, M. Waldow, C. Matheisen, C. Ripperda, J. Bolten, T. Wahlbrin, M. Nagel, F. Merget, and H. Kurz, Opt. Express **19**, 17212 (2011).
9. B. Chmielak, C. Matheisen, C. Ripperda, J. Bolten, T. Wahlbrink, M. Waldow, and H. Kurz, Opt. Express **21**, 25324 (2013).
10. N. Hon, K. Tsia, D. Solli, B. Jalali, and J. Khurgin, *Proceedings of the 6th IEEE International Conference on Group IV Photonics* (IEEE, 2009).
11. A. Grieco, B. Slutsky, and Y. Fainman, "Characterization of waveguide loss using distributed Bragg reflectors," Appl. Phys. B, doi: 10.1007/s00340-013-5543-x (2013).
12. R. Sharipov, "Quick introduction to tensor analysis," arXiv preprint math/0403252 (2004).
13. M. Huang, Int. J. Solids Struct. **40**, 1615 (2003).